

Chapter 2

Tight-Seal Whole-Cell Recording

ALAIN MARTY and ERWIN NEHER

1. Introduction

The tight-seal whole-cell recording method, often abbreviated as “whole-cell recording” (WCR), allows one to record from cells and modify their internal environment by using a patch-clamp pipette. This has become the most commonly used configuration of the patch-clamp technique. In the present chapter, we first describe the basic experimental procedures used to obtain whole-cell recordings. We then discuss the pipette–cell interactions during whole-cell recording, first from an electrical point of view and then from a chemical point of view. We finally compare the tight-seal whole-cell recording with other methods for studying electrical properties of cells.

2. Basic Procedures

To perform whole-cell recordings, patch-clamp pipettes are fabricated and filled with an appropriate low- Ca^{2+} solution. The pipette is pressed onto the cell membrane to establish a “gigaseal” at the contact area. The pipette potential is then changed to a negative voltage (such as 70 mV below the bath potential), and repetitive voltage steps of a few millivolts amplitude are given. At this stage, the fast capacitance compensation is adjusted to cancel the transient caused by the capacitance of the pipette holder and pipette wall (Fig. 1). Pulses of suction are applied to the pipette interior until a sudden increase in the size of the capacitive transients is observed (Fig. 1). This additional current reflects the contribution of the cell membrane to the pipette input capacitance following the destruction of the patch membrane. An alternative but rarely used method to break the patch membrane is to apply to the pipette voltage pulses of large amplitude to induce membrane breakdown (“zapping”). The pulses are very short (e.g., 10–500 μsec) such that once the patch is broken, the cell capacitance does not have the time to be loaded to an appreciable fraction of the applied potential, thus protecting the cell from total dielectric breakdown.

ALAIN MARTY • Neurobiology Laboratory, Teacher’s Training College, École Normale Supérieure, F-75005, Paris, France. ERWIN NEHER • Department of Membrane Biophysics, Max-Planck-Institute for Biophysical Chemistry, Am Fassberg, D-37077 Göttingen, Germany. *Present address For A.M.:* Cellular Neurobiology Workgroup, Max-Planck Institute for Biophysical Chemistry, Am Fassberg, D-37077 Göttingen, Germany

Single-Channel Recording, Second Edition, edited by Bert Sakmann and Erwin Neher. Plenum Press, New York, 1995.

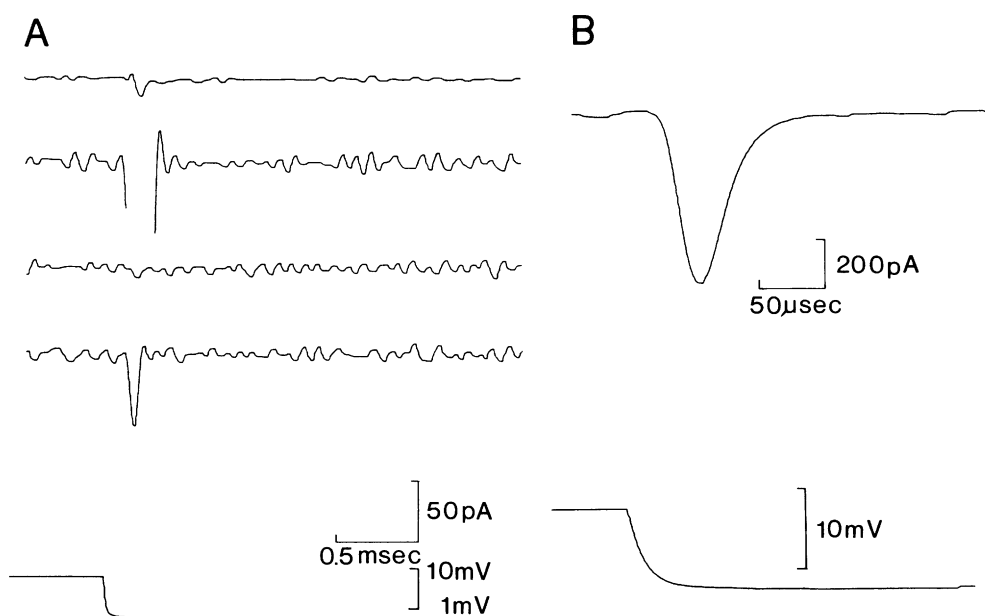


Figure 1. Capacitive currents observed at different stages of WCR. A: The top trace shows the response to a 10-mV voltage pulse after formation of a gigaseal and after cancellation of pipette capacitance, before rupture of the patch. The second trace shows the response to the same stimulus immediately after rupture. The capacitive artifact is off scale; note increase in background noise. The third trace shows the same response after cancellation of cell membrane capacitance (dial settings: $C = 3.56$ pF; $\tau = 20$ μ sec). The fourth trace shows again a response without cell capacitance cancellation, employing a tenfold attenuated stimulus. The lowest trace shows the time course of the voltage pulses. B: Response to a 10-mV hyperpolarizing voltage pulse on a faster time scale (same experiment, WCR without capacitance cancellation).

Once the WCR mode is established, it is often helpful to lift the pipette somewhat to relieve the strain imposed on the cell when the initial seal was established. In some cases, the cell may be lifted further to detach it from the bottom of the recording chamber. In such cases, the solution surrounding the cell can be changed rapidly without impairing the stability of the recording.

Whole-cell recordings can be performed for at least 1 hr without electrical signs of deterioration. (However, as is discussed below, some currents may subside during such long recordings.) Provided that the cell under study is firmly attached to the culture dish, it is then possible to form an outside-out patch simply by pulling away the recording pipette (Hamill *et al.*, 1981). After this maneuver, the cell membrane reseals, leaving the cell essentially intact except that its internal solution has been replaced with the pipette solution. This property can be exploited in several ways. (1) The method may be used to alter the internal solution of a chosen cell with minimal damage to its membrane. (2) Successive WCRs with different internal solutions can be performed on a given cell by changing the recording pipette. (3) Both macroscopic and single-channel data may be obtained in one experiment. It should be noted, however, that the electrical stability of outside-out patches formed after a long WCR is often not as good as that of patches obtained after a few minutes of WCR.

3. The Whole-Cell Recording Configuration from an Electrical Point of View

3.1. The Equivalent Circuit for a Simple Cell

We assume here a reasonably small cell (longest dimension $\leq 100 \mu\text{m}$) with a resistance at rest R on the order of $1 \text{ G}\Omega$ and an input capacitance C on the order of $10\text{--}100 \text{ pF}$. This corresponds to the situation found for a large number of animal cells. This cell is studied using a patch-clamp pipette that has a resistance R_s *during recording* (R_s is different from the pipette input resistance measured before contacting the cell; see below). The equivalent circuit is illustrated in Fig. 2. If V_p , the pipette potential, follows an imposed square impulse of amplitude ΔV , the current I through such a circuit is described by a simple exponential function of time, as illustrated in Fig. 2B. If one assumes that $R_s \ll R$ (typical values are $10 \text{ M}\Omega$ and $1 \text{ G}\Omega$, respectively) one obtains:

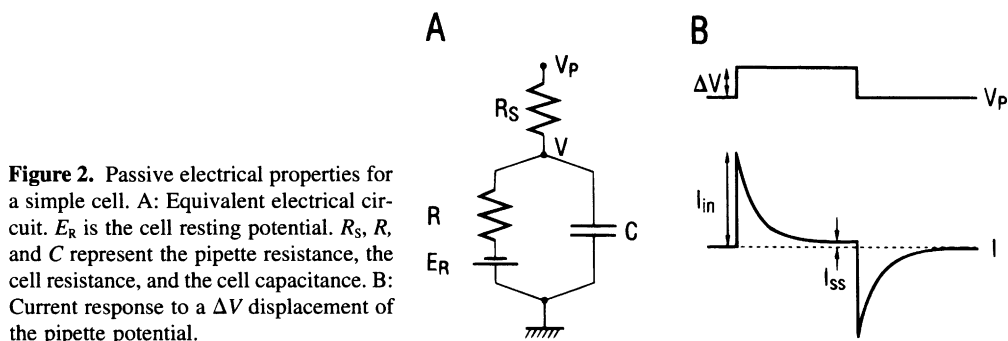
$$I_{\text{in}} = \Delta V / R_s \quad (1)$$

$$I_{\text{ss}} = \Delta V / R \quad (2)$$

and

$$\tau = R_s C \quad (3)$$

Where I_{in} is the “instantaneous current” obtained just after the jump, τ the time constant of the current relaxation, and I_{ss} the steady-state current. I_{in} , I_{ss} , and τ can be all measured from the current record, and equations 1–3 can then be used to calculate R , R_s , and C . Thus, a simple analysis of the current changes recorded in response to a square impulse yields all the parameters of the electrical circuit of the cell but one (E_r , the resting potential of the cell). Note that R_s , as calculated from equation 1, is different from the value found for the resistance of the pipette before making the seal, R_{in} . Typical ratios of R_s/R_{in} are 2–5. If several pulses of suction are applied to the pipette interior, this value can be brought down to 2–3 but not below. This is probably because cytosolic elements impose a lower conductivity to the part of the cell that is sucked into the pipette compared to the conductivity of the bath solution.



3.2. Series Resistance Errors

To illustrate some of the problems associated with series resistance errors, let us assume that we want to measure a Na^+ current in a cell clamped with $R_s = 10 \text{ M}\Omega$. The “ideal” I - V curve is as drawn in Fig. 3A. This is the curve that would be recorded if R_s were zero. For each current value actually recorded, the flow of current along the pipette tip results in a discrepancy between the pipette potential V_p and the cell potential V . According to Ohm’s law $V - V_p = R_s I$. Using this equation, it is possible to predict the distortion brought about by series resistance errors in the I - V curve. A graphic method can be employed to go from the ideal $I(V)$ curve to the experimental $I(V_p)$ curve (or vice versa) as shown in Fig. 3B. As a result of the series resistance error, the $I(V_p)$ curve has a very abrupt take-off near -40 mV , and it reaches its maximum within a few millivolts. In fact, if the maximal slope of the original $I(V)$ curve exceeds 0.1 nA/mV (corresponding to the ratio $1/R_s$), the $I(V_p)$ curve has a jump with infinite slope. The discontinuity occurs as the voltage-clamp system is unable to prevent the cytosolic potential V from firing an action potential. This happens in practice if the maximum I_{Na} current is on the order of 3 nA , a rather modest value. Thus, series resistance errors can severely distort I - V curves. In regions of the curves where the derivative dI/dV is negative, total voltage clamp failure can occur.

A second, potentially serious consequence of the presence of R_s is the fact that, even for large values of R , V does not follow V_p immediately. Thus, if V_p follows a square impulse, V is rounded off with a time constant τ as given by equation 3. With $R_s = 10 \text{ M}\Omega$ and $C = 100 \text{ pF}$, we obtain $\tau = 1 \text{ msec}$. Changes in channel-opening probability can occur much faster than this, for example, during deactivation of Ca^{2+} channels on returning from a depolarized test potential to the holding potential. If, because

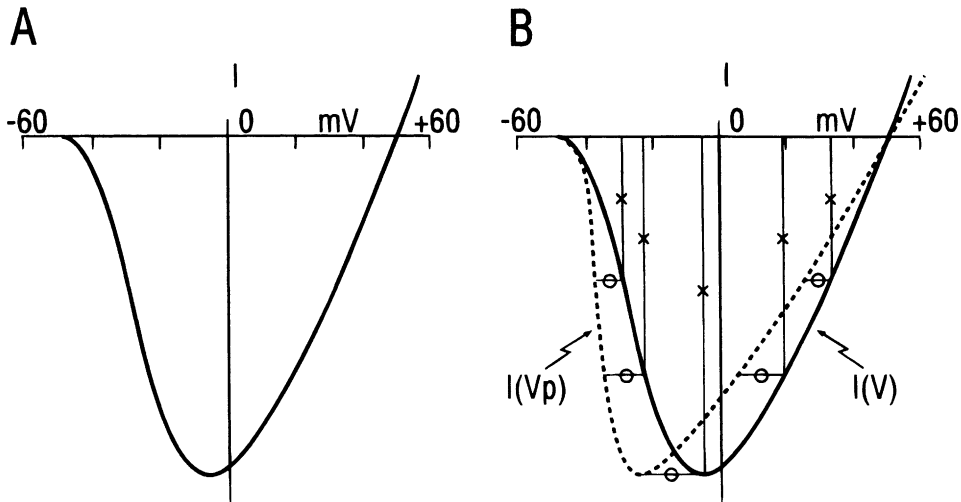


Figure 3. Series resistance errors. A: Assumed ideal I - V curve for peak Na current measurements. B: Because of series resistance errors, the measured curve $I(V_p)$ differs from the ideal curve $I(V)$. It is possible to transform one curve into the other by a graphic method. Here the $I(V) \rightarrow I(V_p)$ transform is illustrated. For all pairs of points the values of the ratio x/o are the same. Note that the $I(V_p)$ curve is much steeper than the $I(V)$ curve in the -40 to -20 -mV voltage range.

of the R_s error, V actually changes with a time constant of 1 msec, such fast processes will have to wait for the changes in V to have occurred, resulting in artifactual changes in the current trace.

Series resistance errors can be dealt with in various ways. To some extent, they can be reduced by series resistance compensation (see below). Residual errors on steady-state currents can be appreciated using the type of transform illustrated in Fig. 3, and I - V curves can be corrected accordingly if R_s is known. Alternative strategies include the use of a single-electrode switching clamp instead of the usual continuous voltage-clamp design.

3.3. Cell Capacitance Cancellation

This should not be confused with series resistance compensation. Capacitance cancellation is performed (1) to avoid saturation of the amplifiers of the recording circuit during the sudden high-amplitude currents generated at the onset of voltage changes and (2) to eliminate error signals caused by the pipette and holder capacitance. In a first step, the small capacitor representing the pipette and pipette holder is canceled at the cell-attached stage. This is called “fast” capacitance cancellation because the time constant of the corresponding current is very fast, in the 0.5- to 5- μ sec range. This first step is essential if one wishes to estimate R_s by using equation 1 once the WCR mode has been established. In WCR, a second cancellation is performed to remove the cell membrane capacitive current. At this stage, most commercial amplifiers display the values of the cell capacitance and access resistance that correspond to the second (slow) capacitive current. Capacitive current cancellation consists of supplying the current needed to charge the capacitor directly to the summing input of the headstage amplifier through a small capacitor C_h (Fig. 4A). To achieve this, an exponentially shaped voltage command is applied to C_h . By adjusting the amplitude and time constant of this voltage V_{shaped} , I_{cap} is made to flow through C_h and not through R_f . It is therefore not recorded. To perform simultaneous cancellation of fast (holder and pipette) and slow (cell) capacitive currents, the sum of two exponentials is fed to V_{shaped} .

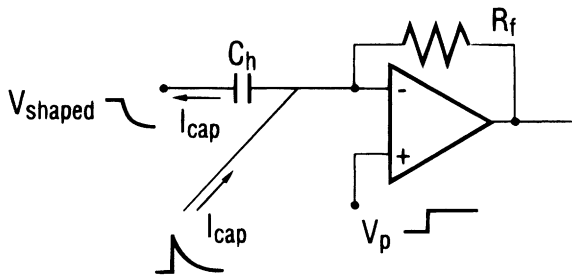
The problem of capacitance cancellation is treated in greater detail in Chapters 4 and 7 (this volume).

3.4. Series Resistance Compensation

The target here is to limit errors in I - V curves and to improve the effective speed of the voltage clamp in order to be able to record fast current changes. The basic idea is to take the current output, scale it with an adjustable gain α , and add the result to the command voltage (Fig. 4B). During voltage pulses, this results in an overshoot of the effectively applied potential (Fig. 5). Also, the system automatically corrects V_p if a sizable ionic current starts to flow. This correction is in essence the inverse of the graphic method used to go from the $I(V)$ curve to the $I(V_p)$ curve in Fig. 3.

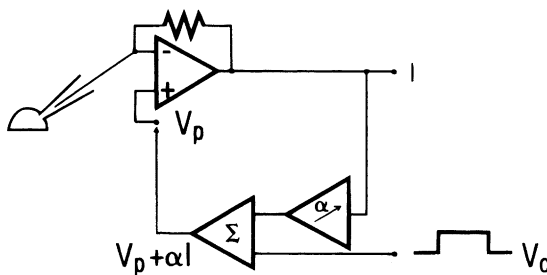
One problem with series resistance compensation is that, because it employs a positive feedback, it can escape control (“ringing”). For this reason it is impossible to reach 100% compensation. Also, the compensation only works if the value of R_s has been determined correctly. R_s may be evaluated by analyzing capacitive current transients

A



capacitive current cancellation

B



series resistance compensation

Figure 4. Cell capacitance cancellation and series resistance compensation. A: Cell capacitance cancellation. At the onset of voltage jumps, an adjustable signal V_{shaped} is fed through a small capacitor C_h to the negative input of the headstage amplifier. The corresponding current flow cancels the capacitive current I_{cap} , such that no net current is recorded by the amplifier. B: Series resistance compensation. The command potential V_p is the sum of the command potential V_c and a signal proportional to the measured current (αI).

using equation 1 or by reading the setting of an appropriately designed capacitance compensation network. Unfortunately, the value of R_s may change spontaneously during recording, thus making later R_s compensations inaccurate. The only way out of this problem is to determine R_s often during the course of the experiment. If R_s increases markedly, it is usually possible to decrease it again, at least transiently, by applying a new pulse of suction to the pipette interior. Computer-controlled patch-clamp amplifiers make it possible to estimate and compensate R_s automatically before each depolarizing voltage pulse.

As an alternative or complement to series resistance compensation, the effective onset of applied potential steps can be accelerated by adding a square pulse of large amplitude and short duration ($\sim 5 \mu\text{sec}$) at the leading edge of command potential steps. The amplitude of the pulse is adjusted empirically in order to minimize the capacitive current transient ("supercharging": Armstrong and Chow, 1987).

Series resistance compensation is usually performed after full cancellation of pipette, holder, and cell membrane capacitive currents (Fig. 5). However, there is no real obligation to proceed that way. Provided that R_s is set at the right value, most commercial amplifiers will perform a correct series resistance compensation (at least for small voltage pulses) in the absence of cell membrane capacitance cancellation. If this is done, however,

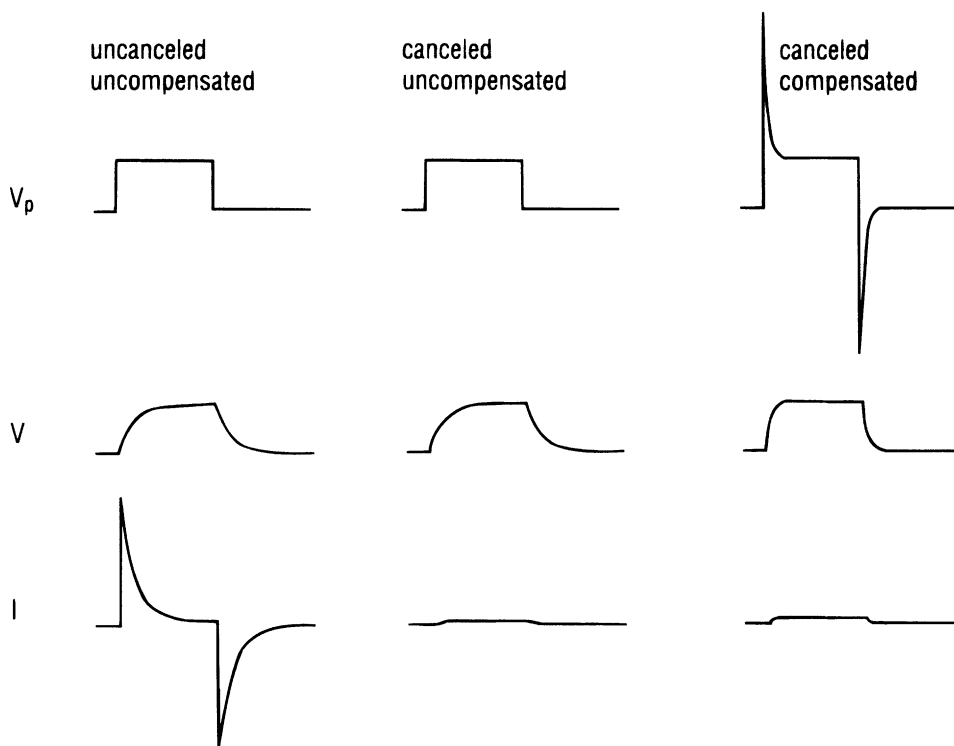


Figure 5. Pipette and cell potential during capacitance cancellation and series resistance compensation. In the uncanceled, uncompensated situation (left column), V_p is rectangular, while V and I are exponential functions of time with the same time constant τ (equation 3). Cancellation of the cell capacitive current does not change the time course of V (middle column). After series resistance compensation, however, V reaches more quickly its steady state (right column). This is achieved by adding an overshooting component to V_p .

capacitive currents will saturate quickly for increasing pulse amplitudes, as series resistance compensation results in faster and larger capacitive currents. Saturation of capacitive currents will delay effective voltage-clamp control.

3.5. Capacitance Cancellation Together with Series Resistance Compensation

When both techniques are employed, the problem arises that capacitance cancellation eliminates part of the current, which does not appear past the first amplifier. As a result, the gain in voltage-clamp speed expected from series resistance compensation during voltage pulses may be lost. Fortunately, this problem can be fixed by adding again the signal corresponding to the capacitive current to the recorded current at the end of the recording chain when shaping the correction voltage that is added to the command potential (more details on this problem can be found in Chapter 4, this volume).

3.6. Current Clamp

Current-clamp measurement can be performed with the same basic circuit with an additional feedback loop. The loop connects the current output to the command input of the pipette potential and provides negative feedback for constant-current operation, as described by Sigworth (Chapter 4, this volume).

The same procedure should be used to effectively subtract the pipette and holder capacitance as in voltage-clamp recordings. If this is not done, voltage signals following current steps will be artificially slowed down.

3.7. Noise

The dominating source of background noise in a whole-cell recording is likely to be the membrane capacitance C in series with the access resistance R_s . The power spectrum $S(f)$ of such a combination is given by

$$S(f) = 4kTR_s(2\pi fC)^2/[1 + (2\pi fR_sC)^2]$$

For typical values of R_s and C (see above), this term is much higher than the noise of the membrane conductance over most of the frequency range of interest. This is documented in Fig. 6, which shows the noise power spectra of two bovine adrenal chromaffin cells.

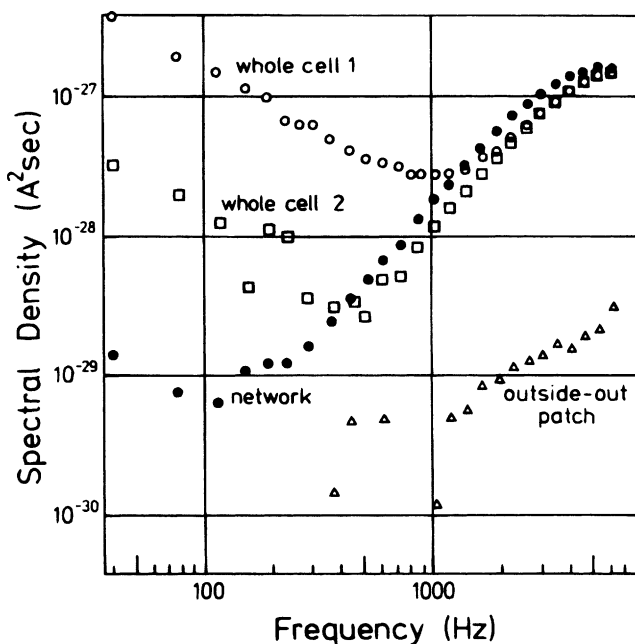


Figure 6. Average noise-power spectra of different recording situations. Power spectra of current records were taken from two adrenal chromaffin cells in the whole-cell configuration. Both cells were bathed in standard saline containing 15 μ M TTX. Each had a membrane capacitance between 5.7 and 5.8 pF and a series resistance of about 5.2 M Ω . The latter value was calculated from the time constant of the capacitive current and from the cell membrane capacitance. In the recordings from cell 1, the pipette was filled with a Cs⁺-containing internal solution, and the holding potential was zero. During the recording of cell 2, the pipette was filled with a K⁺-containing internal solution, and the cell was held at -70 mV. For comparison, the power spectrum of a resistor-capacitor network with the following values is shown: series resistance 5.2 M Ω , capacitance 5.85 pF, parallel resistance 8.5 G Ω .

When the pipette was withdrawn from cell 1, an outside-out patch formed. Its noise power spectrum is included in the figure. A background noise spectrum (including amplifier and pipette holder noise as well as noise from the tape recorder on which the data were temporarily stored) was subtracted from the whole-cell and outside-out spectra. This control was obtained from a recording with a pipette mounted onto the amplifier but not immersed in solution. The spectrum of the resistor-capacitor network was corrected for the noise of the open-input amplifier. All curves are averages of 300 individual spectra.

Both cells had a spectral density rising with the square of the frequency above 1 kHz and saturating between 5 and 10 kHz according to the above equation. The power spectrum of a resistor-capacitor network with similar parameters is shown for comparison. Cell 1 was held at 0 mV and had appreciable noise attributable to ionic channels, which dominates the noise power below 1 kHz. Still, in the range 40 Hz to 1 kHz, the noise from the series combination R_sC is ten times larger than the conductance noise (the logarithmic display distorts the relative contributions). Cell 2, which was held at -70 mV under more “physiological” conditions, was very quiet. Noncharacterized single-channel inward currents (Fenwick *et al.*, 1982b, Fig. 21) at low frequency could be observed; their noise dominated the power spectrum at frequencies below 400 Hz.

All spectral densities measured in the whole-cell configuration are one to two orders of magnitude higher than those measured with patches. For comparison, a spectrum from an outside-out patch is also shown Fig. 6. It was measured on a patch taken from cell 1 after completion of the whole-cell measurements.

The background noise of cell 2 corresponds to an rms value of 0.15 pA in the frequency range 0 to 400 Hz and to approximately 1.5 pA_{rms} for 0 to 4 kHz. Thus, single channels of relatively long duration (such as ACh-induced channels) can be well resolved in a whole-cell recording (see Fenwick *et al.*, 1982a), whereas short single-channel events (such as Na⁺ channels) are lost. Still, the dynamic range of such a measurement is remarkable. This is illustrated in Fig. 7, which shows Na⁺ currents in response to depolarizing voltage pulses in a chromaffin cell at 3.5-kHz bandwidth. The left column shows the response to various small depolarizations (from -70 mV holding) at a relatively sensitive current scale. Discrete fluctuations caused by individual Na⁺ channels can be seen in the uppermost record, but they are not clearly resolved. As the membrane is depolarized further, these fluctuations add up to sizable, highly fluctuating currents. In the right column, traces from larger depolarizations are shown, but at a ten-times-smaller current scale. On this scale, the background fluctuations are no longer visible (see segments before pulses); maximum inward currents rise to 1400 pA, which is approximately 600 times the rms noise of background.

3.8. Equivalent Circuit for a Complex Cell

Some cells cannot be described by the simple equivalent circuit of Fig. 2. Brain neurons, for example, have complicated dendritic arborizations that are not instantly charged if a square voltage pulse is applied to the soma. Cerebellar Purkinje cells are a good example. In these neurons, the capacitive current response to a hyperpolarizing voltage pulse is the sum of two exponentials. In such a case capacitive current cancellation of the fast component can be performed as illustrated in Fig. 8. Series resistance compensation leads to an acceleration of the time constant of decay of the slow component. The situation can be modeled with a two-compartment equivalent circuit (Fig. 8). The first compartment, with potential V_1 , is represented by the soma and proximal dendrites. The second compartment, with potential V_2 , corresponds to the main part of the dendritic tree. At the onset of the voltage pulse, V_1 follows a double exponential with time constants τ_1 and τ_2 , whereas V_2 follows a single exponential (after a short delay) with time constant τ_2 . After series resistance compensation V_1 follows a step function, but V_2 remains an exponential function of time. However, the time constant of this exponential, τ'_2 , is shorter than τ_2 . The acceleration of V_2 can be followed by monitoring the canceled capacitive current trace. It can be shown that τ'_2 is also the time constant of filtering

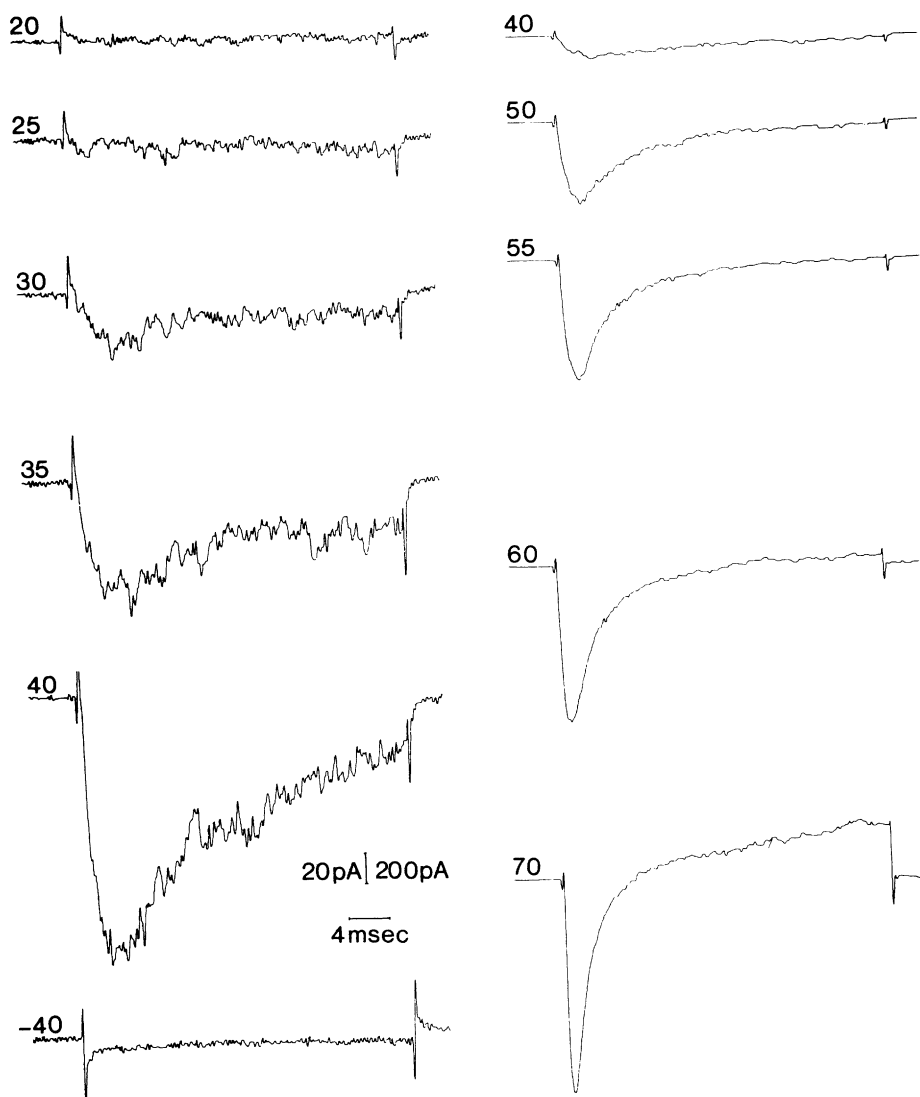


Figure 7. Dynamic range of current measurement in the whole-cell clamp. Sodium currents from a chromaffin cell with membrane capacitance of 5.8 pF ($R_s = 5 \text{ M}\Omega$) were elicited by depolarizing pulses of various amplitudes (given in millivolts at the start of each trace); holding potential was -70 mV . Current amplitudes cover the range from the single-channel level ($\approx 2 \text{ pA}$) to 1400 pA ; 3.5-kHz bandwidth; 21°C . The bath contained normal physiological saline; the pipette was filled with a K^+ -containing internal solution. A hyperpolarizing response is shown in the left lower corner. It shows a biphasic residual capacitive artifact resulting from a slight imbalance of the τ setting in the capacitive cancellation network. Following that, a slow capacitive component is seen, which carries approximately $10 fC_b$, corresponding to 0.4 pF . A large part of this component probably arises from the pipette, because isolated patches or sealed pipettes show similar artifacts. The largest currents in this figure are subject to clamp errors of approximately 7 mV .

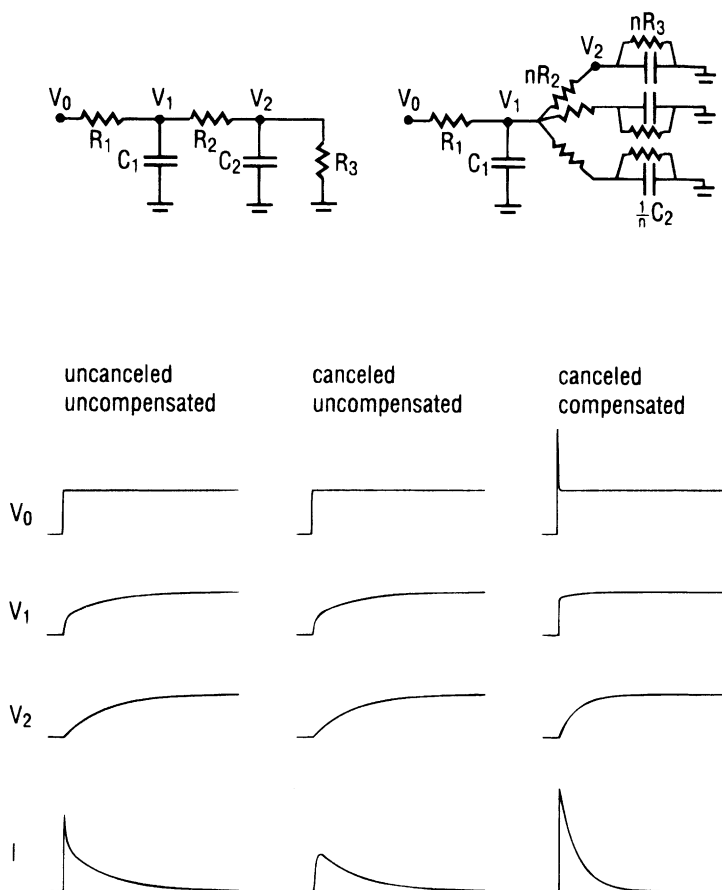


Figure 8. Capacitive currents in Purkinje cells. Upper panels: Two-compartment equivalent circuit modeling the passive properties of cerebellar Purkinje cells. V_0 is the pipette potential, and R_1 the pipette resistance. The first compartment (soma and proximal dendrites) is at a potential V_1 . It has an infinite membrane resistance and a capacitance C_1 . The second compartment (distal dendrites) is at a potential V_2 . It has a resistance R_3 and a capacitance C_2 . In the scheme on the right, the second compartment has been subdivided into n equivalent subcompartments representing individual branches of the dendritic tree. The two variants of the equivalent circuit are not distinguishable in somatic recordings. Lower panels: Capacitive current responses for the two-compartment equivalent circuit. The upper traces represent the potential V_0 applied to the pipette; the next traces show the voltage transients in compartments 1 and 2; the lower trace shows the capacitive current. In the uncanceled, uncompensated situation, V_1 is the sum of two exponential functions of time, with time constants τ_1 and τ_2 . V_2 rises after a short delay with the slower time constant τ_2 . I is biphasic, with time constants τ_1 and τ_2 . In the recording that was used to make the calculations, τ_1 and τ_2 were 0.26 and 4.51 msec (Llano *et al.*, 1991, Fig. 2). From the time constants and amplitude ratio of the capacitive current the following values were calculated: $R_1 = 8.9 \text{ M}\Omega$, $R_2 = 5.6 \text{ M}\Omega$, $C_1 = 76 \text{ pF}$, $C_2 = 311 \text{ pF}$. Capacitive current cancellation was performed by removing the fast component of the capacitive current, as shown in the middle traces, without any gain in the speed of voltage control. Series resistance compensation of resistance R_1 (right) led to a substantial acceleration of V_1 and V_2 . Note the overshoot of V_0 . Calculations show the effect of 90% compensation. The slow time constant takes the new value $\tau'_2 = 2.0 \text{ msec}$.

of dendritic signals originating in compartment 2 (Llano *et al.*, 1991). Thus τ'_2 represents the limitation of effective voltage control introduced by dendritic filtering.

Whereas Purkinje cells can be satisfactorily modeled with a two-compartment equivalent circuit, other neurons cannot. In hippocampal pyramidal cells, for instance, three exponentials are needed to model the capacitive current decay. In such complex cases a cable analysis may be more appropriate than a multicompartment model (Jackson, 1992).

4. The Whole-Cell Recording Configuration from a Chemical Point of View

4.1. Modeling Diffusion between Pipette and Cell Compartments

Whole-cell recording establishes simultaneously an electrical and a chemical pathway to the cell interior. It is obviously desirable to determine to what extent, and at which speed, do pipette and cell contents equilibrate. Given the prevailing volume ratio ($\sim 10 \mu\text{l}$ for the pipette and $\sim 1 \text{ pl}$ for the cell), it is clear that eventually the pipette solution will dictate the concentration of all diffusible substances. However, the time of equilibration may vary greatly depending on the exact cell geometry and on the size of the diffusible substance. The only rigorous approach to this problem is to apply the equations of diffusion to the geometry of the pipette–cell assembly. This can be done by dividing this assembly in a number of compartments, as illustrated in Fig. 9A, and by solving the diffusion equations in each compartment (Oliva *et al.*, 1988). We consider below an alternative solution to the problem, which has the advantage of highlighting the parameters that determine the speed of diffusion.

4.2. A Solution for a Two-Compartment Model

To simplify calculations, one can assume two homogeneous compartments separated by a transition zone where concentration gradients occur. The first of these compartments

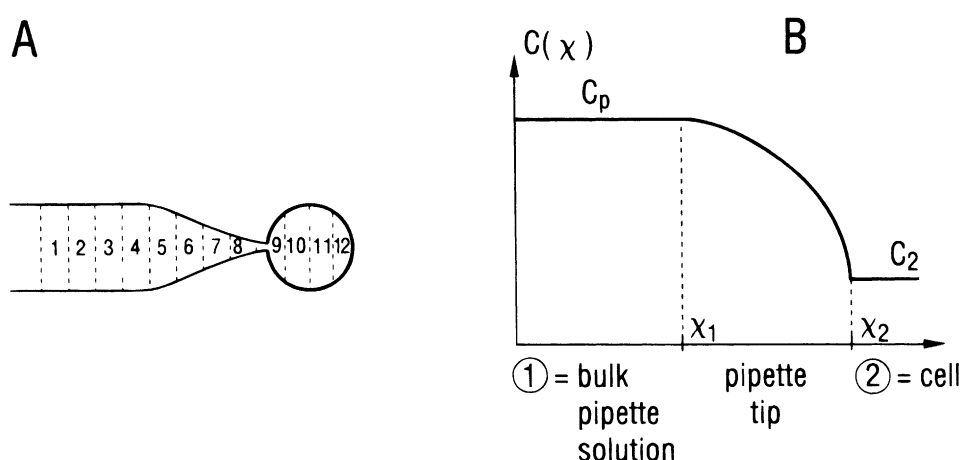


Figure 9. Pipette–cell equilibration. A: A multicompartment model of the pipette–cell assembly. B: Simplified diffusion model with two compartments separated by a transition zone representing the pipette tip.

is the bulk of the pipette solution, where the original concentration c_p of a given substance stays constant simply because the pipette volume is so much larger than the cell volume. At the other end of the diffusion path, the concentration c_2 of this substance in the cell may also be considered homogeneous. This is because concentration gradients can dissipate much faster in the cell (typical diameter $\geq 10 \mu\text{m}$) than in the pipette tip (inner diameter $\sim 1 \mu\text{m}$). Compartments ① and ② are linked by a resistive region represented by the pipette tip (Fig. 9B). During the loading process of the cell c_2 evolves from its original value c_0 to the final value c_p . To simplify the calculations, we further assume that diffusion is a steady-state process in the sense that accumulation of the diffusing substance in the pipette tip can be neglected. The following derivation can then be made, after Mathias *et al.* (1990).

Let us consider the diffusion process in the pipette tip. According to Fick's law the flux of diffusing substance at position x is

$$\Phi(x) = -D \, dc(x)/dx \quad (4)$$

where D is the diffusion constant of the substance, and $c(x)$ is the concentration at position x . By definition, the flux is the ratio of the amount transferred at position x , $J(x)$, to the cross-section area of the pipette in x , $A(x)$:

$$\Phi(x) = J(x)/A(x) \quad (5)$$

$J(x)$ is independent of x , because we assumed that the substance is transferred at the same time through all x positions of the pipette tip without accumulation anywhere but in compartment ②. Thus, $J(x) = J$.

Finally, the resistance of the pipette tip is the sum of elementary resistances represented by slabs of fluid of area $A(x)$ and length dx :

$$R_s = \int_{x_1}^{x_2} \frac{\rho}{A(x)} \, dx \quad (6)$$

where ρ is the resistivity of the pipette solution. Combining equations 4 and 5 yields

$$-D \, dc(x)/dx = J/A(x)$$

By integration from $x = x_1$ to $x = x_2$, we obtain

$$D[c(x_1) - c(x_2)] = J \int_{x_1}^{x_2} \frac{dx}{A(x)}$$

Combining with equation 6 yields

$$D[c(x_1) - c(x_2)] = (J/\rho) R_s$$

Now $c(x_1) = c_p$, and $c(x_2) = c_2$. Therefore,

$$c_p - c_2 = \frac{J R_s}{D \rho} \quad (7)$$

Since J is the flux to compartment ②,

$$J(x) = J = v \frac{dc_2}{dt}$$

where v is the cell volume. Combining with equation 7 yields

$$\frac{dc_2}{dt} = \frac{Dp}{R_s v} (c_p - c_2). \quad (8)$$

The solution to this differential equation is an exponential function of time with a time constant

$$\tau = R_s v / Dp \quad (9)$$

Equation 9 shows that the time constant of equilibration of a substance is proportional to the cell volume and to the pipette resistance and inversely proportional to the diffusion coefficient of this substance. Some of these predictions have been tested. In chromaffin cells, Pusch and Neher (1988) have shown that, inasmuch as R_s remained constant, the time course of equilibration of a variety of fluorescent compounds was exponential. For an R_s value of 10 M Ω , time constants of exchange varied from about 4 sec (for K⁺) to 1 min for substances of molecular weight around 1000. Furthermore, in conformity to equation 9, equilibration times were inversely proportional to the diffusion coefficient D and proportional to the pipette resistance R_s . From their data a value of 240 Ω cm is calculated for the pipette resistivity by using equation 9. This is about fourfold higher than the resistivity of the pipette solution. The results suggest that the effective resistivity of the cytoplasm sucked into the pipette tip is about four times higher than that of the bath solution. This is in line with the above-mentioned result that the ratio R_s/R_{in} of the pipette access resistances measured in the bath and during WCR is at best of the order of 2 to 3.

4.3. Extension to Multicompartment Cells

The above analysis reveals an analogy between the speed of voltage changes and that of diffusion. In both cases the equilibrium is reached, for a round cell, as an exponential function of time. In both cases the time constant of the exponential is proportional to R_s (see equations 3 and 9). The analogy can be extended to more complex cases. Thus, the two-compartment model of Fig. 8 predicts not only a two-exponential capacitive current but also a two-exponential loading curve during pipette-cell equilibration. In the latter case, the time constants of loading are a function of the series resistances R_1 and R_2 , of the diffusion constant of the diffusing substance, and of the volumes v_1 and v_2 of the two compartments. Approximate values for the time constant t_1 and t_2 of equilibration may be obtained provided that equilibration proceeds faster in the first compartment than in the second ($R_1 v_1 \ll R_2 v_2$).

$$t_1 = v_1/[D\rho(1/R_1 + 1/R_2)]$$

$$t_2 = v_2(R_1 + R_2)/D\rho$$

(The equation for t_2 reduces to equation 9 in the case that $R_1 = 0$.)

This is to be compared with the corresponding values of the decay time constants of the capacitive current under similar assumptions ($R_1C_1 \ll R_2C_2$) (Llano *et al.*, 1991, equations 1 and 2):

$$\tau_1 = C_1/(1/R_1 + 1/R_2)$$

$$\tau_2 = C_2/(R_1 + R_2)$$

For each compartment, the capacitance is thus replaced by the ratio $v/D\rho$.

4.4. Pipette Filling Solutions for WCR

A standard pipette solution for whole-cell recording contains a pH buffer (e.g., 10 mM HEPES, adjusted to pH 7.4), a Ca buffer (e.g., 10 mM EGTA + 1 mM Ca, giving $Ca_i \approx 10$ nM), MgATP (~ 2 mM; in order to have ATPases active), free Mg^{2+} (~ 1 mM, as a cofactor for many cytosolic processes). GTP (~ 0.1 mM) is included in cases where processes involving G proteins are studied. ATP and GTP are poorly stable. Pipette solutions should therefore be kept frozen when they contain either nucleotide. During experiments, thawed solutions should be kept on ice. For long-duration (>30 min) recordings, it is advisable to use an ATP-regenerative system in order to obviate ATP degradation in the recording pipette. Because cells normally contain millimolar concentrations of glutathione, a reducing agent, one probably should (but often one neglects to do so) include ~ 5 mM glutathione as well. Inactivation of K^+ (Ruppersberg *et al.*, 1991) and Na^+ channels (Strupp *et al.*, 1992) depends on the redox potential of the internal solution and will be abnormal unless glutathione is duly supplemented.

The standard intracellular anion is Cl^- . In cases where it is desired to keep a negative equilibrium potential for Cl^- , a large fraction of the internal Cl^- is replaced by an impermeant ion. Glutamate, MOPS, and isethionate are often used for this purpose. F^- is also used as an intracellular anion. It is often permeant through Cl^- permeable channels. The advantage of F^- over Cl^- is that seal formation and recording stability are often better. However, F^- ions make complexes with traces of Al^{3+} , leading to the formation of AlF_4^- , a potent activator of G proteins. F^- ions also act as Ca^{2+} buffer, so that they may interfere with Ca-dependent processes. Thus, the use of F^- is inappropriate for the study of signaling pathways involving G proteins or intracellular messengers.

4.5. Perforated Patch Recording

It often occurs that an important cell function disappears during whole-cell recording as a result of the loss of unknown diffusible factors into the recording pipette ("washout"). One solution to this problem is to establish the electrical connection between cell and pipette not by suction, but by incorporation of a channel-forming substance in the cell-

attached mode (“perforated patch”). There is no washout if the critical diffusing molecule is unable to cross the exogenous channel (Fig. 10A). Nystatin, a polyene antibiotic with antifungal profile, is commonly used for this purpose (Horn and Marty, 1988; Korn *et al.*, 1991). This choice was derived from the following properties of nystatin channels (Kleinberg and Finkelstein, 1984, and references herein). (1) They are 8 Å in diameter. Molecules larger than this (mol. wt. ≥ 300) do not pass through. (2) They are permeable to all small monovalent cations and anions (however the permeability is larger for cations than for anions; $P_{\text{Na}}/P_{\text{Cl}} \sim 10$). This makes it possible to control the internal K^+ , Na^+ , and Cl^- concentrations, which are equal to the pipette solution values after a few minutes of recording. Cs^+ can be readily substituted for K^+ if one wishes to block K^+ currents. Ca^{2+} ions are not permeant. (3) They are not voltage dependent. This ensures a good behavior of the recording system when the command (pipette) potential is changed.

Nystatin inhibits the formation of seals; it is therefore important to fill the pipette tip with a nystatin-free solution, while the rest of the pipette is filled with nystatin-containing solution (Fig. 10B). Filling the pipette tip with nystatin-free solution is achieved by dipping the pipette for ~ 2 sec into that solution. Then the shank of the pipette is

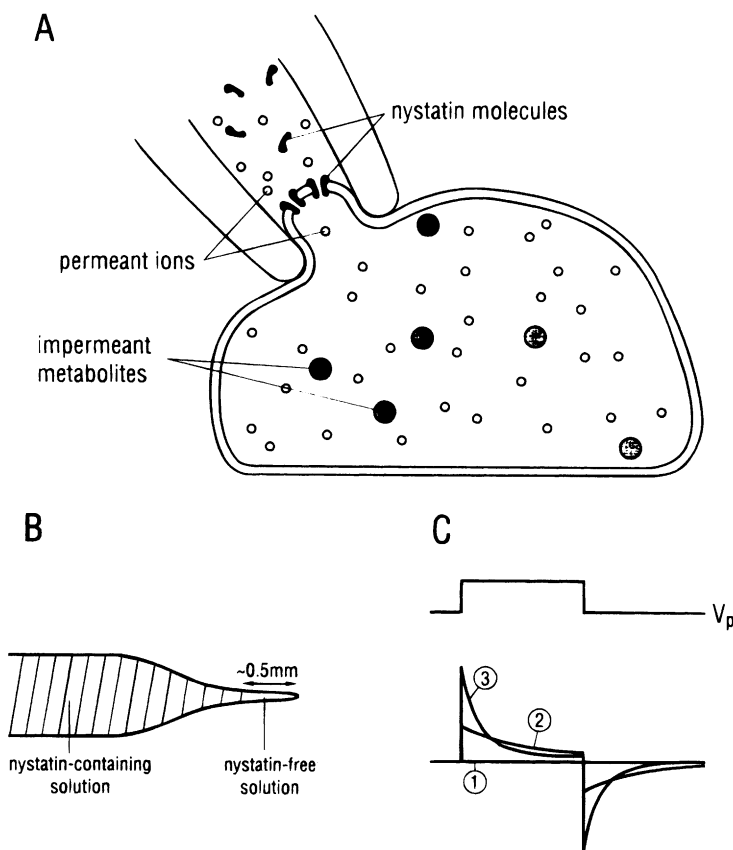


Figure 10. Perforated patch recording. A: Diagram illustrating the principle of the method. B: Pipette-filling procedure for perforated patch recording. C: Schematized current responses to voltage pulses during establishment of perforated-patch recording.

filled from the back with nystatin-containing solution. Bubbles can be removed in the usual way by gently tapping the pipette held upright. Practice has shown that this does not eliminate the nystatin-free region. Once the pipette is filled, it is secured in the pipette holder and approached to the cell in the usual manner. Two points have to be kept in mind at this stage, however. First, only very modest pressure should be applied to the pipette interior in order to avoid premature filling of the pipette tip with nystatin. Second, the approach should be fairly rapid for the same reason. Constant perfusion of the bath is helpful in avoiding accumulation of nystatin during the approach. Making the seal proceeds as usual by applying gentle suction to the pipette interior. As nystatin diffuses to the pipette tip, it gradually increases the pipette–cell conductance. This process can be conveniently monitored by observing current response to repetitive voltage steps (Fig. 10C). One should record sequentially responses such as ①, ②, and ③. The whole process may take 2–10 min. In ①, there are no nystatin channels in the patch. In ② and ③, there is an electrical communication between cell and pipette, so that the cell capacitor is loaded by the voltage jumps. The situation is the same as that described in Fig. 2, except that R_s should be replaced with the resistance R_p of the patch of membrane with its nystatin channels. (In fact, the resistance is $R_s + R_p$, because both resistances are in series. But R_p is usually 5 or 10 times larger than R_s , so that it is the predominant term.) Equation 3 can then be rewritten as $\tau = R_p C$. Thus, as R_p decreases during the course of the incorporation of nystatin channels, τ decreases (②→③). At the same time I_{in} increases, as predicted by equation 1.

Nystatin is a poorly water-soluble substance that tends to aggregate. It also has a series of double bonds, which makes it very sensitive to light. In view of these properties, the following precautions are mandatory. First, sonication is required both to make the nystatin stock solution (usually 50 mg/ml in DMSO) and the final pipette solution (final nystatin concentration 100 μ g/ml). Second, the stock and pipette solutions have to be protected from light carefully. During recording, the microscope light should be turned off whenever it is not required.

Other substances can be used instead of nystatin. Amphotericin B, another polyene antibiotic, is structurally close to nystatin and can be used in a similar manner (Rae *et al.*, 1991). ATP is able to permeabilize certain cells by opening channels. It was used inside of patch pipettes in the earliest version of perforated patch recording (Lindau and Fernandez, 1986). Some specific recipes and rules for handling nystatin and amphotericin solutions are given by Zhou and Neher (1993) and in Chapter V of the *Axon Guide* (Sherman-Gold, 1993).

The ratio R_s/R_{in} of the series resistance during perforated-patch recording to the initial pipette resistance is usually 10–20, e.g., substantially larger than in standard WCR. This results in a comparatively slow voltage clamp. However, one advantage of perforated patch recordings is that the value of R_s is very stable, thus allowing a more reliable series resistance compensation than in standard WCR.

4.6. Changes in Effective Membrane Voltage during WCR

During WCR, potential changes occur at the pipette–cell junction and at the cell membrane. These changes arise from several mechanisms, which are reviewed in this section. They elicit “voltage shifts” in functionally important curves, such as activation or inactivation curves of voltage-dependent currents.

4.6.1. Liquid Junction Potentials

Liquid junction potentials, i.e., potential differences between two solutions, occur at all boundaries between solutions of differing compositions. They result from the charge separation that occurs when anions and cations of different mobilities diffuse across boundaries. With physiological solutions the magnitude of such junction potential ranges from a few up to about 12 mV.

In WCR particular attention has to be paid to the junction potential existing at the tip of the recording pipette because the pipette filling solution usually is not the same as the bath solution. Before seal formation the liquid junction at the tip typically is that of a K^+ -rich solution in the pipette against physiological saline in the bath. If KCl is the predominant salt in the pipette, then the liquid junction potential is only about 3 mV, the pipette being negative with respect to the bath. If, however, a larger anion is selected, such as in a K^+ -glutamate-based pipette filling solution, the anion will lag behind in the diffusion such that the pipette will be negative by about 10 mV. This is relevant for subsequent WCR measurement because it is standard practice to null the pipette current in this situation by adjusting a variable offset, so that the amplifier reads both zero current and zero voltage at the beginning of the measurement while the pipette interior actually is at -10 mV. In the WCR configuration, however, the liquid junction and the concentration gradients at the pipette tip no longer exist, particularly after diffusional equilibration between the cell interior and the pipette (for details see below). Then, the pipette potential and the cell interior will still be at -10 mV when the amplifier reads zero voltage. Therefore, all voltage readings of the amplifier have to be corrected by this amount. This correction is commonly referred to as the “liquid junction potential correction.”

Liquid junction potentials can either be determined experimentally (Neher, 1992) or calculated from the generalized Henderson equation (Barry and Lynch, 1991). A computer program for calculating the corrections and illustrating their use is described by Barry (1993). The most difficult part is to convince oneself of the sign of the correction. Different strategies of handling the liquid junction potential correction and other offset problems are given in Chapter 6 (this volume). Provided that the bath solution is normal saline, the rule of thumb for WCR measurements is that the actual membrane potential is more negative than the amplifier reading if the dominant anion of the pipette filling solution is less mobile than the dominant cation, and vice versa for a less mobile cation.

4.6.2. Donnan Equilibrium Junction Potential

Junction potentials exist at any interfaces between different solutions and also at the interface between pipette solution and cytoplasm. However, the gradual exchange of ions between pipette and the cell interior may cause a gradual drift in this junction potential. Let us assume that the exchange of small ions (e.g., K^+ and Cl^-) is very fast compared to that of proteins and polyanions. After equilibration of the small ions, the pipette–cell system constitutes a Donnan equilibrium with an excess of immobile particles in the cell (the proteins and polyanions). We assume that these particles are negatively charged, so that the cell potential V_i is more negative than the pipette potential V_0 . As the particles diffuse out of the cells (a process that may last many minutes, see above), the difference between V_0 and V_i subsides.

The pipette concentration of the cation (say K^+) at the onset of the protein exchange is given by the Boltzmann equation:

$$[K]_i = [K]_0 \exp(-V/U) \quad (10)$$

with $U = 25$ mV and $V = V_i - V_0$. Likewise, the initial concentration of the small anion (say Cl^-) is

$$[Cl]_i = [Cl]_0 \exp(V/U) \quad (11)$$

In addition, electrical neutrality requires that

$$[Cl]_0 = [K]_0 \quad (12)$$

and

$$[K]_i = [P]_i + [Cl]_i \quad (13)$$

where $[P]_i$ is the number of fixed charges (in Faradays) per liter.

Equations 10 to 13 give

$$u^2 + ([P]_i/[K]_0)u - 1 = 0 \quad (14)$$

with $u = \exp(V/U)$.

This last equation in u allows us to calculate V as a function of $[P]_i$ and $[K]_0$. In the extreme case in which all negative charges of the cell are immobile, $[P]_i = [K]_0$, and one finds $V = -12$ mV. In actual cases, however, $[P]_i$ is smaller than $[K]_0$, and V is accordingly smaller.

In summary, we expect the membrane potential to be more negative than the clamp potential at the beginning of the experiment. The difference V should be at most 12 mV and should gradually decline with a time course of minutes. Liquid junction potentials of approximately this magnitude were found to occur at the tip of conventional glass microelectrodes when filled with isotonic saline (Hironaka and Morimoto, 1979).

Figure 11 shows the results of an experiment designed to test these predictions. The pipette potential was held at -100 mV throughout the experiment. Sodium currents were measured at different times after the beginning of the WCR. Both peak-current and h_∞ curves showed a negative shift after 30 min of WCR (Fig. 10B). In Fig. 10C, the shift of the activation curve (compared to the curve obtained 1 min after WCR) is plotted as a function of time. The shift reached 9 mV in 30 min. Similar results were obtained in other experiments. Signs of a negative voltage shift were also found in the analysis of Ca^{2+} currents (see Fenwick *et al.*, 1982b, Fig. 17). In addition, we found in a previous study of Na^+ currents that a negative shift of 10–15 mV occurs rather quickly (within 1 or 2 min) just after formation of an outside-out patch (Fenwick *et al.*, 1982b). This shift is probably of the same nature as that illustrated in Fig. 11. The fact that it occurs more quickly for an outside-out patch than in a WCR is consistent with the view that it is linked to a diffusion process. In a Donnan equilibrium, permeant ions are at equilibrium, i.e., have a homogeneous electrochemical potential. Therefore, the above voltage shift does *not* apply for the reversal potentials of ion-selective pathways. Thus,

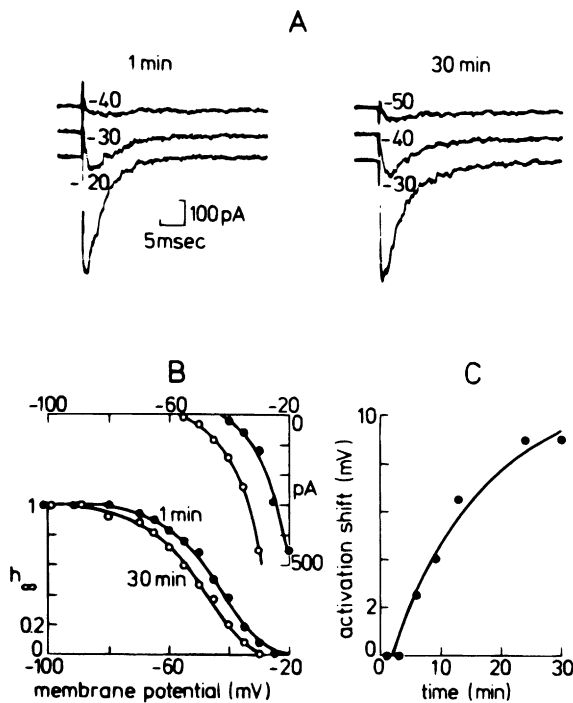


Figure 11. Slow potential shift in WCR. The pipette solution contained 140 mM KCl. The bath contained normal saline except that Ca^{2+} ions were replaced by Co^{2+} to eliminate Ca^{2+} currents. Positive pulses were given at 0.5 Hz from a holding potential of -100 mV. The amplitudes of the resulting Na^{+} currents were measured at various times after the start of the WCR (taken as $t = 0$). Also h_{∞} curves were obtained by measuring the current at -15 mV following an inactivating pulse 40 msec long. A: Currents at -40 , -30 , and -20 mV after 1 min of recording (left) and at -50 , -40 , and -30 mV after 30 min of recording (right). The two sets of records indicate a 10 mV negative voltage shift. B: Peak current (above) and h_{∞} (below) curves obtained at 1 min (●) and 30 min (○). The curves indicate a negative shift of 9 mV and 6 mV, respectively. C: Voltage shift of the activation curve as a function of time. The shift was measured at the 300-pA level with comparison to the curve obtained at $t = 1$ min. The curve may be approximated by an exponential having a time constant of about 15 min. Cell capacitance $C = 5.4$ pF. Time constant of capacitive current $\tau = 25$ μsec .

in the case of Na^{+} channels, the activation and inactivation curves are shifted, but the reversal potential is maintained.

It should be pointed out, however, that shifts along the voltage axis may occur from other effects. Thus, during the course of WCR, membrane proteins may undergo phosphorylation/dephosphorylation as a result of inevitable changes in cytosol composition. Such processes can change the apparent potential "felt" by these proteins according to the additional change of phosphate residues. Since these residues are negatively charged, the activation and inactivation curves of the phosphorylated channel are shifted toward positive potentials (Perozo and Bezanilla, 1990). In frog skeletal muscle, shifts in the activation curve of Na^{+} channels were found to depend on the nature of anions, following the lyotropic series (Dani *et al.*, 1983).

5. Comparison of Whole-Cell Recording with Other Electrophysiological Methods to Record from Cells

Initially it was thought that a major limitation of WCR was that the requirement to form a tight seal necessitated a perfectly clean cell membrane. Many physiological preparations, where the cell of interest is covered by other cells or by extracellular material, seemed out of range. Recently, however, procedures have been developed that largely overcome this limitation (see Chapter 8, this volume). In view of these developments the comparison of WCR with traditional microelectrode recordings has gained some new interest.

In bovine chromaffin cells, WCR measurements give an input resistance of 1–10 G Ω and a resting potential of about –60 mV (Fenwick *et al.*, 1982a). This compares with values of up to 500 M Ω and about –60 mV with microelectrodes (Brandt *et al.*, 1976). Thus, WCR gives a higher resting resistance than conventional recordings. A similar discrepancy is often found in other preparations. It is often argued that the larger conductance seen with microelectrodes is genuine, because an artifactual leak conductance should bring the apparent resting potential close to 0 mV, whereas recorded resting potentials are similar with the two methods. Therefore, the low conductance seen in WCR is attributed to the loss of a physiologically important conductance as a result of washout. But this hypothesis is unlikely in chromaffin cells because the low input conductance is observed immediately on establishment of WCR, i.e., before any substance could have left the cell. Furthermore, the input conductance is similar in standard WCR and in perforated patch recording. As an alternative to the washout hypothesis, it can be proposed that the discrepancy is in fact caused by a leakage conductance around the site of impalement in microelectrode recordings. Along the leakage pathway, Ca ions enter the cell, where they activate Ca-dependent K channels. The combination of the additional Ca-dependent K conductance and the depolarizing leakage conductance yields an input conductance much larger than in WCR although the measured resting potentials are similar.

Recent WCR results in central neurons likewise yield input resistance values much larger than previous microelectrode measurements (e.g., hippocampal granule cells: Edwards *et al.*, 1989; Staley *et al.*, 1992; cerebellar Purkinje cells: Llano *et al.*, 1991). Such large values may have important functional implications. In a situation of low background synaptic activity, individual synaptic signals arising at distant dendritic locations will be effectively propagated to the soma by simple electrotonic spread. Such signals can therefore initiate a somatic action potential without requiring active propagation along the dendrite (Stuart and Sakmann, 1994).

References

- Armstrong, C. M., and Chow, R. H., 1987, Supercharging: A method for improving patch-clamp performance, *Biophys. J.* **52**:133–136.
- Barry, P. H., 1993, JP Calc, a software package for calculating liquid junction potential corrections in patch-clamp, intracellular, epithelial and bilayer measurements and for correcting junction potential measurement, *J. Neurosci. Methods* **51**:107–116.
- Barry, P. H., and Lynch, J. W., 1991, Liquid junction potentials and small cell effects in patch-clamp analysis, *J. Membr. Biol.* **121**:101–117.
- Brandt, B. L., Hagiwara, S., Kidokoro, Y., and Miyazaki, S., 1976, Action potential in the rat chromaffin cells and effects of acetylcholine, *J. Physiol.* **263**:417–439.
- Dani, J. A., Sanchez, J. A., and Hille, B., 1983, Lyotropic anions. Na channel gating and Ca electrode response, *J. Gen. Physiol.* **81**:255–281.
- Edwards, F. A., Konnerth, A., Sakmann, B., and Takahashi, T., 1989, A thin slice preparation for patch-clamp recordings from neurones of the mammalian central nervous system, *Pflügers Arch.* **414**:600–612.
- Fenwick, E. M., Marty, A., and Neher, E., 1982a, A patch-clamp study of bovine chromaffin cells and of their sensitivity to acetylcholine, *J. Physiol.* **331**:577–597.
- Fenwick, E. M., Marty, A., and Neher, E., 1982b, Sodium and calcium channels in bovine chromaffin cells, *J. Physiol.* **331**:599–635.
- Hamill, O. P., Marty, A., Neher, E., Sakmann, B., and Sigworth, F. J. 1981, Improved patch-clamp techniques for high-resolution current recording from cells and cell free patches, *Pflügers Arch.* **391**:85–100.
- Hironaka, T., and Morimoto, S., 1979, The resting membrane potential of frog sartorius muscle, *J. Physiol.* **297**:1–8.

- Horn, R., and Marty, A., 1988, Muscarinic activation of ionic currents measured by a new whole-cell recording method, *J. Gen. Physiol.* **94**:145–159.
- Jackson, M. B., 1992, Cable analysis with the whole-cell patch-clamp. Theory and experiment, *Biophys. J.* **61**:756–766.
- Kleinberg, M. E., and Finkelstein, A., 1984, Single-length and double-length channels formed by nystatin in lipid bilayer membranes, *J. Membr. Biol.* **80**:257–269.
- Korn, S. J., Marty, A., Connor, J. A., and Horn, R., 1991, Perforated patch recording, *Methods Neurosci.* **4**:264–273.
- Lindau, M., and Fernandez, J. M., 1986, IgE-mediated degranulation of mast cells does not require opening of ion channels, *Nature* **319**:150–153.
- Llano, I., Marty, A., Armstrong, C. M., and Konnerth, A., 1991, Synaptic- and agonist-induced excitatory currents of Purkinje cells in rat cerebellar slices, *J. Physiol.* **434**:183–213.
- Mathias, R. T., Cohen, I. S., and Oliva, C., 1990, Limitations of the whole cell patch clamp technique in the control of intracellular concentrations, *Biophys. J.* **58**:759–770.
- Neher, E., 1992, Correction for liquid junction potentials in patch-clamp experiments, *Methods Enzymol.* **207**:123–131.
- Oliva, C., Cohen, I. S., and Mathias, R. T., 1988, Calculation of time constants for intracellular diffusion in whole cell patch clamp configuration, *Biophys. J.* **54**:791–799.
- Perozo, E., and Bezanilla, F., 1990, Phosphorylation affects voltage gating of the delayed rectifier K⁺ channel by electrostatic interactions, *Neuron* **5**:685–690.
- Pusch, M., and Neher, E., 1988, Rates of diffusional exchange between small cells and a measuring patch pipette, *Pflügers Arch.* **411**:204–211.
- Rae, J., Cooper, K., Gates, G., and Watsky M., 1991, Low access resistance perforated patch recordings using amphotericin B, *J. Neurosci. Methods* **37**:15–26.
- Ruppersberg, J. P., Stocker, M., Pongs, O., Heinemann, S. H., Frank, R., and Koenen, M., 1991, Regulation of fast inactivation of cloned mammalian $I_K(A)$ channels by protein phosphorylation, *Nature* **352**:711–714.
- Sherman-Gold, R. (ed.), 1993, *The Axon Guide*, Axon Instruments, Inc., Foster City, CA.
- Staley, K. J., Otis, T. S., and Mody, I., 1992, Membrane properties of dentate gyrus granule cells: Comparison of sharp microelectrode and whole-cell recordings, *J. Neurophysiol.* **67**:1346–1358.
- Strupp, M., Quasthoff, S., Mitrovic, N., and Grafe, P., 1992, Glutathione accelerates sodium channel inactivation in excised rat axonal membrane patches, *Pflügers Arch.* **421**:283–285.
- Stuart, G. J., and Sakmann, B., 1994, Active propagation of somatic action potentials into neocortical pyramidal cell dendrites, *Nature* **367**:69–72.
- Zhou, A., and Neher, E., 1993, Mobile and immobile calcium buffers in bovine adrenal chromaffin cells, *J. Physiol.* **469**:245–273.

<http://www.springer.com/978-1-4419-1230-5>

Single-Channel Recording

Sakmann, B.; Neher, E. (Eds.)

1995, XXII, 700 p. 52 illus., 2 illus. in color., Softcover

ISBN: 978-1-4419-1230-5